

## Infrared Thermal Signature Evaluation of a Pure Ice Block

Taimur Rashid, Hassan A. Khawaja, K. Edvardsen

Department of Engineering and Safety  
The Arctic University of Norway (UIT)  
Tromsø, Norway  
e-mail: taimur.rashid@uit.no

Umair N. Mughal

Department of Industrial Engineering  
Narvik University College (HIN)  
Narvik, Norway  
e-mail: unum@hin.no

**Abstract**—Marine operations in cold climates are subjected to heavy ice accretion, which can lead to heavy ice loads causing safety concerns. Atmospheric and sea spray icing can cause severe ice accretion on structures. Ice detection over the relatively larger surface area of marine platforms and vessels could be significant for ice mitigation and its removal in cold climates. A thermal ice signature can be considered a useful property that could be detected using the Infrared (IR) cameras. To study this remote ice detection option, preliminary lab experimentation was performed to detect thermal gradients over two different surface areas of a pure ice sample at room temperature. A complete thermal signature over the surface area was detected and recorded until the meltdown process was completed. The proposed technique can be useful in detecting ice over large areas in cold marine environments than point detection ice sensing. However, challenges remains in terms of the validation of the detection signature and elimination of false detection.

**Keywords**- icing; infrared; thermal signature; cold region.

### I. INTRODUCTION

Ice accretion problems are challenging in the cold climate regions. With a rise in activity in the arctic frontier, icing phenomena will increasingly affect operational activities. The sources of icing may vary according to environmental conditions, for instance atmospheric icing (snow, rain, fog) [1] or sea spray icing generated due to wind or wave-structure collision [2]. In marine icing events, combination of the mentioned causes could also be the case. An example of this is the snow that sticks to a wet surface caused by the sea spray. All of the discussed factors can cause heavy ice accumulation on offshore and mobile platforms operating in the cold climates [3]. Adequate measures are required to minimize the influence of atmospheric and sea spray icing events on structures under different conditions and, therefore, effective anti/de-icing techniques become important [4]. These techniques involve thermal, chemical and mechanical methods to avoid and/or remove the ice [5]. Most often the problem arises in situations where unpredicted or unexpected environmental conditions occur that could cause heavy ice accretion phenomena, as the ice accretion rate is high enough to become a possible threat to the structure. In such cases the time elapsed becomes the critical factor in responding in an effective manner, which also includes ice mitigation and removal. A viable option available is timely ice detection over the structure during heavy icing events, which should support the anti/de-icing systems. Timely detection can be

important to the mitigation of heavy ice loads upon structures.

In this paper a brief insight into the concept of infrared (IR) thermography is given in Section II. Suitable wavelengths to detect cold objects with infrared detectors is also discussed. Section III gives the details about the preliminary experimentation performed to evaluate the IR thermal signature of a pure ice block and the results are discussed in Section IV. Also included is a brief discussion on remote IR detection in marine operations, which will be the applicability of this research project followed by the concluding remarks in Section V.

### II. IR THERMOGRAPHY AND THERMAL SIGNATURE DETECTION AT LOW TEMPERATURES

IR light is electromagnetic radiation with a wavelength longer than that of visible light, measured from the nominal edge of visible red light at  $0.74\mu\text{m}$  and extending conventionally up to  $300\mu\text{m}$ . Figure 1 shows the IR spectral band that is generally sub-divided into four sub-bands; near infrared (NIR) ranges between  $0.75\text{--}1\mu\text{m}$ , shortwave infrared (SWIR) is from  $1\text{--}2.5\mu\text{m}$ , middle infrared (MWIR) is between  $3\text{--}5\mu\text{m}$ , longwave infrared (LWIR) is between  $8\text{--}14\mu\text{m}$ .

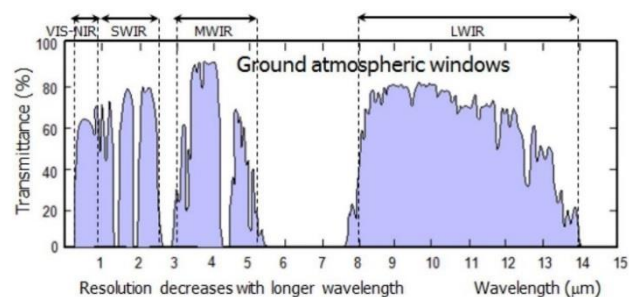


Figure 1. IR Spectrum [6]

For cold objects near  $0^{\circ}\text{C}$ , the prominent radiation wavelength is near  $11\mu\text{m}$ . Since most commercial IR sensors use wavelengths between  $8\text{--}14\mu\text{m}$ , IR thermography can be handful for surface ice studies [7]. Theoretically, each body at any temperature above absolute zero will emit some radiation, but the intensity and frequency distribution of the radiation is different based on the basic structure of the body.

The energy emitted by a true blackbody is the maximum theoretically possible for a given temperature. The radiative power (or number of photons emitted) and its wavelength distribution are given by the Planck’s radiation law (given by (1) and (2)), where  $\lambda$  is the wavelength,  $T$  is the temperature,  $h$  is Planck’s constant,  $c$  is the velocity of light, and  $k$  is Boltzmann’s constant.

$$\frac{2\pi hc^2}{\lambda^5} [\exp(\frac{hc}{\lambda KT}) - 1]^{-1} W / (cm^2 \mu m) \tag{1}$$

$$P(\lambda, T) = \frac{2\pi c}{\lambda^4} [\exp(\frac{hc}{\lambda KT}) - 1]^{-1} photons / (scm^2 \mu m) \tag{2}$$

Figure 2 shows a plot of these curves for a number of blackbody temperatures. With a rise in temperature, the energy emission at any given wavelength increases respectively and the wavelength of peak emission decreases, which is specified by Wien’s displacement law. The waveband 1–15  $\mu m$  in the IR region of the electromagnetic spectrum contains the maximum radiative emission for thermal imaging purposes.

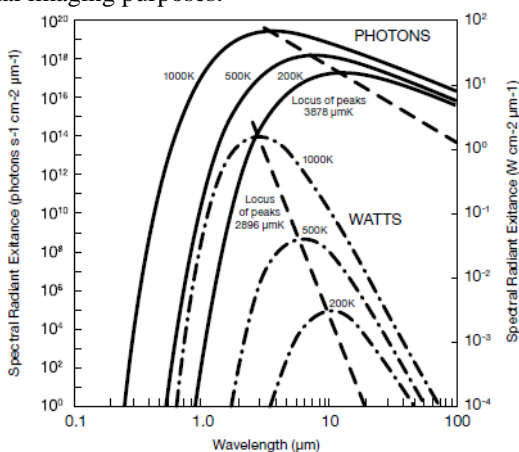


Figure 2. Spectral radiance excitance (Planck’s Law) [8]

The working principle of an IR camera is based on thermography imaging. The major components of the camera are lens, detector, video processing electronics and user interface control. The incident beam of light is focused by the lens upon the detector. The detector contains the IR sensitive elements arranged in the array called focal plane array (FPA). These are IR sensitive elements and miniature in size (micrometers). The resolution of FPA determines the resolution of the IR imagery produced by the camera. Many IR cameras available have user interface to calculate the scene temperature along with imagery recording software. Calibration is often required to read out the correct temperature across the scene that is captured.

With the advancement in the IR camera-technology, significant work has been done to observe ice/snow emissive properties to support remote microwave detection. Snow and clear ice have high emissivity values, which makes them

convenient to thermally image. Snow emissivity has been variously found to be 0.98 for frost [9], above 0.98 for small-grained snow under 1000  $\mu m$  [10], 0.96 for flat solid ice and water, and as low as 0.8 for old snow. Measurements obtained at particular wavelengths (e.g. 10  $\mu m$ ) have observed emissivity as high as 0.995. Conversely, the thermal reflectance of snow  $r$  is less than 2.3% between the 4 to 14  $\mu m$  wavelengths [11]. This holds good for various snow types including granular, fine, wet, and dry; whereas newly fallen snow reflectance is less than 1% between 4 to 14 $\mu m$ . For most of the 7.5 to 13 $\mu m$  spectrum, the emissivity is found higher in comparison. Therefore, IR cameras operating in the range above 7.5 $\mu m$  can prove significant to observe cold objects.

### III. PURE ICE BLOCK THERMAL SIGNATURE

In order to test the potential of IR ice detection, it is necessary to evaluate the thermal signature of icing. In order to observe the IR signature of pure ice, lab experimentation was performed. The sample was prepared from freezing tap water in a commercial freezer. The dimension of the ice block prepared was 14.5 x 14 x 5.5 cm. Although the dimensions were randomly chosen, it was taken into consideration that the ice block should have a large enough surface area to allow observation of a differentiating thermal signature and a wide range of temperature profiles. As a starting point, the viewing angle of the IR camera and the ice sample was kept at 90 degrees. The forward-looking IR camera FLIR A310 was used to observe the thermal signature of the block using the proprietary software of the FLIR device. The observations acquired were produced in the mentioned calibrated software. FLIR A310 series IR camera has a detector operating in the range of MWIR (8-11 $\mu m$ ). The thermal signature was recorded immediately from the time when sample was taken out of the freezer. The observations were recorded until the melt-down phenomena had started at room temperature and surface of the ice block acquired a uniform temperature.

The lab setup performed is shown in the Figure 3. An attempt was made to observe a freely suspended ice block in order to ensure the uniform heat transfer from all directions. To hold the ice block on the stand, a wooden piece was immersed into the cold water during freezing process, so that it could be used as a suspension support assisted by a clamping stand as shown in Figure 3. Minimal thermal conduction from the ice block was expected from the wooden support (since the wood has poor conductivity), apart from fulfilling the suspension support requirement. The ice block was initially frozen to approximate -26°C and suspended on the stand immediately after taking out of the freezer and observed from IR camera. FLIR A310 has an uncooled detector device that sends IR frames processed at the rate of 5Hz. The FLIR calibrated software acquires the frames and saves them as a sequence file. The camera to software communication is performed via an Ethernet protocol. The IR image of the larger surface-1 and relatively smaller surface-2 (Figure 3) was recorded at room temperature to evaluate the surface temperature profiles.

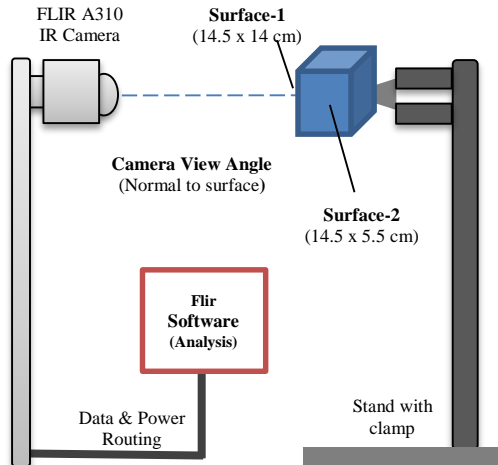


Figure 3. Lab setup of pure ice block thermal signature evaluation

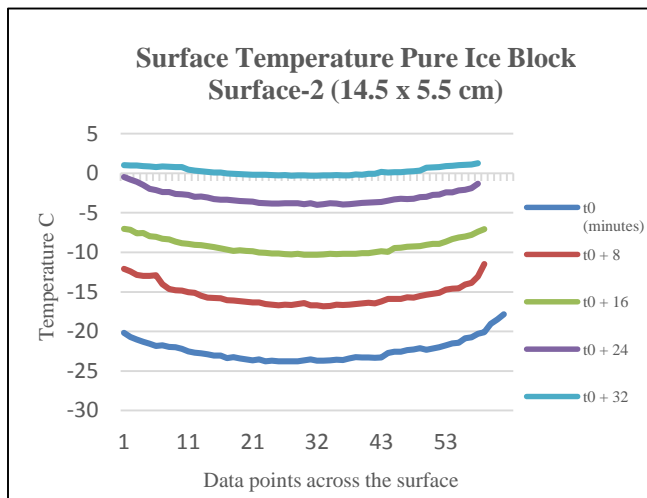
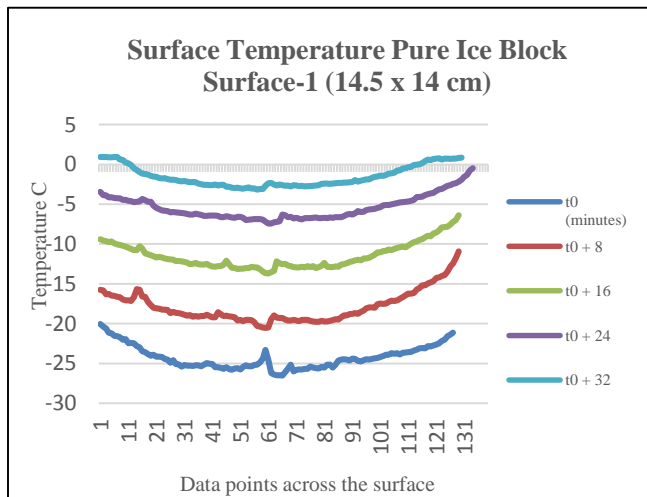


Figure 4. Surface temperature of Ice block recorded from thermal IR signature at different intervals till meltdown starts

The temperature observations were made along a linear path along the ice block’s centre line to capture the maximum thermal gradient across the surface. This helped to acquire the maximum and minimum temperature profiles over the surfaces 1, 2 (Figure 4). Minimum temperatures of  $-26.5^{\circ}\text{C}$  for surface-1 and  $-23.7^{\circ}\text{C}$  for surface-2 were recorded. The gradual rise in temperature for both the surfaces was observed simultaneously as the heat transfer process took place at room temperature. The observations for surface-1 are noted after regular intervals of time  $t_0$  to  $t_0+32$  and also simultaneously for surface-2 as shown in Figure 4. The thermal IR signature available from the camera optics was captured during the course of the observations, which presents the distribution of the thermal profile as shown in Figure 5. The lowest temperature profile was observed almost at the centre of the ice block surfaces whereas the maximum temperature at the boundaries.

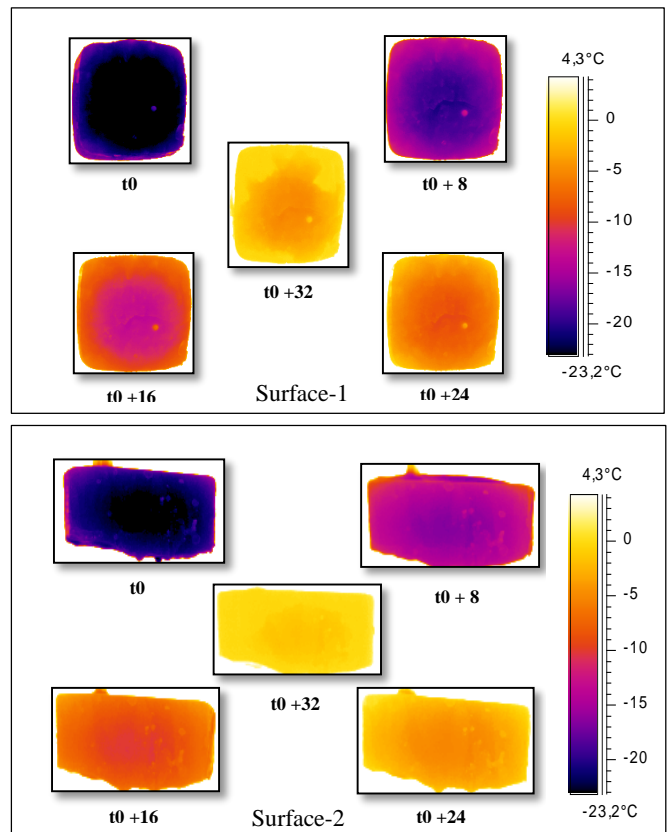


Figure 5 Thermal IR signature distribution across surface

#### IV. DISCUSSION

Pure ice has a high emissive value and it produces a distinguishable thermal signature shown in Figure 5. The ice block suspended through the wooden stick allowed the ice to conduct heat uniformly. The IR observations show the thermal gradient from the centre of the ice block towards the outside, which follows the heat transfer process. The heat conduction through the boundary layer of the ice can be easily identified from the thermal signatures as shown in

Figure 5. The minimum temperature at surface-1 is  $-26.5^{\circ}\text{C}$  at  $t_0$  (Figure 4), which is located in the geometric centre of the surface. A similar behaviour is observed at surface-2. In terms of the maximum temperature profile at the boundary layers, not much difference was observed between both the surfaces. The highest temperature of  $0.92^{\circ}\text{C}$  was observed at the boundary of surface-1 at  $t_0$  as compared to the  $1.1^{\circ}\text{C}$  of surface-2 shown in Figure 4. The maximum-minimum difference in the two surface areas was noted as surface-1 has wider span of temperature range as compared to the surface-2 possibly because of the larger surface area. The maximum-minimum temperature difference at time  $t_0$  to  $t_0+32$  for surface-1 was  $6.44^{\circ}\text{C}$ ,  $9.61^{\circ}\text{C}$ ,  $7.32^{\circ}\text{C}$ ,  $6.98^{\circ}\text{C}$  and  $4.07^{\circ}\text{C}$  respectively. At similar time intervals ( $t_0$  to  $t_0+32$ ) for surface-2, the difference between maximum and minimum temperature recorded was  $5.99^{\circ}\text{C}$ ,  $5.24^{\circ}\text{C}$ ,  $3.2^{\circ}\text{C}$ ,  $3.2^{\circ}\text{C}$  and  $1.59^{\circ}\text{C}$ . The temperature profiles of the ice block can be correlated with the isothermal images shown in the Figure 5. In the IR image of both the ice surfaces the difference in thermal signature can also be observed at the boundary layer of the ice block, which is at a higher temperature as compared to the rest of the surface block. The temperature profile decreases from corners to the centre of the ice block. Since the room temperature was uniform throughout the experiment, it can be safely said that maximum heat transfer occurred from the boundary through natural convection.

It is to be noted that the wide range of the IR profile of the pure ice block also assists in differentiating it with a relatively hotter environment, though in a cold climate environment this may not be the scenario. IR detection for colder objects seems to work well as long as thermal non-uniformity is present in the scene which is to be observed. Currently, offshore structures and marine ships operating in cold environment use thermal methods for anti/de-icing, apart from other methods. Thermally active heated floors will generate a predictable IR signature. Ice accretion on the floors may result in different thermal signature. This variation may be used for ice detection and may also lead to the detection of the ice accretion rate if used in conjunction with heat transfer theory.

## V. CONCLUSIONS

The thermal signature of icing can be applied to detect cold objects especially ice accreted upon the structures. The lab experimentation shows the thermal signature and gradient of two surface areas of a pure ice block. The results shown are preliminary and only reflect the changes in temperature due to warming of ice block under room temperature. LWIR FLIR A310 camera can be used to monitor IR signature of ice. Study of ice block showed that temperature varies over time with maximum value at the boundaries and minimum at the centre. The difference between the boundary and the centre temperatures is higher on a larger surface area. The influence of emissivity values on ice detection is not discussed here and needs to be further investigated.

Considering marine arctic operations, an IR imaging device is to be tested and advanced experimentation is needed to be performed to validate the ice detection and growth.

## ACKNOWLEDGEMENTS

The work reported in this paper is funded by the MAROFF, project no. 195153/160 in collaboration with Faroe Petroleum. We would also like to acknowledge the support given by Prof. James Mercer at University of Tromsø.

## REFERENCES

1. Fikke, S., Cost 727: atmospheric icing on structures. Measurements and data collection on icing: State of the Art, Publication of MeteoSwiss, 2006. 75(110): p. 1422-1381.
2. Makkonen, L., Salinity and growth rate of ice formed by sea spray. Cold Regions Science and Technology, 1987. 14(2): p. 163-171.
3. Ryerson, C.C., Ice protection of offshore platforms. Cold Regions Science and Technology, 2011. 65(1): p. 97-110.
4. Farzaneh, M. and C.C. Ryerson, Anti-icing and deicing techniques. Cold Regions Science and Technology, 2011. 65(1): p. 1-4.
5. Ryerson, C.C., Icing Management for Coast Guard Assets. 2013, Engineering Research and Development Center, Cold regions research and engineering lab: Hanover NH.
6. Dhar, N.K., R. Dat, and A.K. Sood, Advances in Infrared Detector Array Technology. Optoelectronics - Advanced Materials and Devices. 2013.
7. Rees, W.G., Remote sensing of snow and ice. 2005: CRC Press.
8. Rogalski, A., Infrared detectors: an overview. Infrared Physics & Technology, 2002. 43(3): p. 187-210.
9. Wolfe, W.L. and G.J. Zissis, The infrared handbook. Arlington: Office of Naval Research, Department of the Navy, 1978, edited by Wolfe, William L.; Zissis, George J., 1978. 1.
10. Dozier, J. and S.G. Warren, Effect of viewing angle on the infrared brightness temperature of snow. Water Resources Research, 1982. 18(5): p. 1424-1434.
11. Salisbury, J.W., D.M. D'Aria, and A. Wald, Measurements of thermal infrared spectral reflectance of frost, snow, and ice. Journal of Geophysical Research: Solid Earth (1978–2012), 1994. 99(B12): p. 24235-24240.